ACS APPLIED POLYMER MATERIALS

pubs.acs.org/acsapm

Article

Two-Dimensional Triazine Polymers as Recyclable Fluorescent Sensors to Detect and Remove Sub-nanomolar Hg(II) From Water

Maryam Salahvarzi, Mohsen Adeli,* Ebrahim Mehdipour, and Mohammad Nemati

Cite This: ACS Appl. Polym. Mater. 2024, 6, 11750−11761

Read Online

ACCESS | Metrics & More | Article Recommendations | Supporting Information

ABSTRACT: In this work, full triazine two-dimensional frameworks ($2DC_3N_3$) were synthesized and used to detect metal ions in aqueous solutions. $2DC_3N_3$ showed excellent performance to sense Hg(II) with high selectivity (>96%) and was designed as a recyclable sensor for Hg(II) detection. $2DC_3N_3$ was synthesized using catalyst-free [2+2+2] cyclotrimerization of sodium cyanide and cyanuric chloride at ambient conditions. The as-prepared $2DC_3N_3$ sheets with several hundred micrometers lateral size exhibited strong excitation-dependent fluorescence with 63% quantum yield and maximum emission at 428 nm. The emission of $2DC_3N_3$ decreased with 14.74×10^3 L·mol^{-1} quenching constant (K_{SV}) upon interaction with Hg^{2+} ions. This effect was used as a strong signal to detect Hg(II) with a 0.98 nM detection limit. The high Hg^{2+} removal capacity of $2DC_3N_3$ was attributed to cooperative interactions of nitrogen atoms of $2DC_3N_3$ pores and Hg^{2+}, as suggested by computational studies. Taking advantage of the straightforward synthesis of $2DC_3N_3$ and its selectivity, it can be used as an efficient platform for monitoring Hg^{2+} in waste and drinking water.

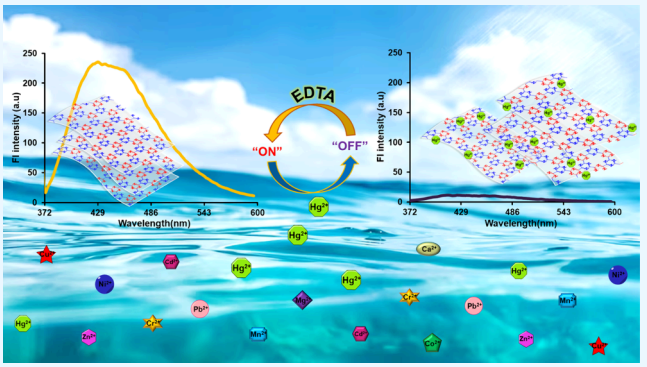

KEYWORDS: *Recycling, Covalent triazine frameworks, Two-dimensional frameworks, Fluorescence sensor, Hg(II) sensing*

INTRODUCTION

Heavy metal ion pollution has become a crucial worldwide challenge due to its bad effects on environmental and public health.[1] Metal ions, because of their high toxicity and bioaccumulation in the environment, can cause severe diseases and destructive effects on ecosystems even at very low concentrations.[2] Among various elements and divalent cations, mercury ion (Hg^{2+}) is known as an infectious heavy metal ion and is listed as a precedence-controlled pollutant by the World Health Organization.[3] Exposure to Hg^{2+} as a pollutant in water and the environment leads to serious health risks including brain, liver, and kidney damage as well as central nervous system and immune system dysfunction. It can also cause various psychiatric and cognitive and motion disorders.[4] Therefore, synthesis of new materials with the ability of efficiently and selectively sensing heavy metals ions as well as rapid and cost-effective removal of these ions is of high importance and interest.[5,6] In recent years, the sensitive detection and efficient removal of metal ions have been investigated and realized by different platforms including supramolecular polymers,[7] metal organic frameworks (MOFs),[8,9] metal−phenolic nanomaterials (MPNs),[10] carbon nanomaterials (CNMs),[11,12] covalent organic frameworks (COFs)[13] and covalent triazine frameworks (CTFs).[14] COFs are stable platforms with excellent physicochemical properties. However, their optical properties are not of high interest. Their layers show a high affinity to stack on each other, leading to strong quenching of fluorescence and weak optical signals.[15] Moreover, current synthetic methods, which are mostly based on protocols at high temperatures, result in defected and carbonized structures with poor optical properties.[16] In addition, the low water dispersibility of such platforms deteriorates their fluorescent and hampers their sensing applications.[17] In previous reports, two-dimensional triazine covalent organic frameworks, due to their predesigned structure, unique photoluminescence and good biocompatibility, porous structures and high surface area, are excellent candidates for sensing and removing pollutants.[18,19] In the present study using different monomers, two-dimensional triazine covalent organic frameworks with various morphologies, particle size, topological connectivity, water dispersibility, regular periodic pore structures, excellent chemical and thermal stability, and tunable functionality can be synthesized.

Full triazine frameworks (C_3N_3) with a large number of heteroatoms and strong noncovalent interactions with other

Received: June 10, 2024
Revised: September 12, 2024
Accepted: September 17, 2024
Published: September 27, 2024

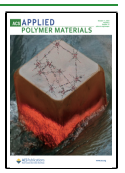

molecules are potentially promising materials for both selective recognition and efficient removal of harmful metal ions from the environment.[20,21] To achieve strong photoluminescence sensing and fast and efficient monitoring of heavy metal ions, the porous polytriazines were selected not only for their specific surface coordination with Hg^{2+} but also for their stability and reusability of the materials.[22] Therefore, they should be investigated to sense metal ions including Hg^{2+}, which is vitally important in the areas of public health, food and beyond.[23] Most importantly, due to the presence of nitrogen rich atoms in the ordered structure of $2DC_3N_3$, that have excellent adsorption sites for Hg^{2+}, significant fluorescent quenching without changing the wavelength occurs upon interaction with Hg^{2+} ions, which is comparable with the previously reported frameworks.[24,25]

Several procedures have been proposed for the production of C_3N_3 frameworks,[26] which require high temperatures and metal catalysts,[27] thus leading to undefined and carbonized structures with low reproducibility. In order to produce a C_3N_3 framework with a two-dimensional topology and defined repeating units, new protocols based on straightforward reactions at low temperatures, convenient operation, low cost, and high accuracy are required to minimize defects and carbonization. One of the main approaches for the construction of aromatic compounds and heterocyclic rings is [2+2+2] cyclotrimerization of alkynes at ambient conditions.[28,29] In this regard, we have developed a metal directed and solvent mediated protocol[30] and a new method for the [2+2+2] polymerization of multifunctional monomers with ethynyl substituents without using any catalyst[31] through which we have been able to produce two-dimensional triazine frameworks with defined structures. Recently, we developed our catalyst-free [2+2+2] cyclotrimerization to monomers bearing carbonitrile for the production of $2DC_3N_3$.[32] The reaction between cyanuric chloride and sodium cyanide at low temperature followed by in situ cyclotrimerization at ambient conditions resulted in $2DC_3N_3$s.

In this work, we report on the synthesis and application of $2DC_3N_3$ for the fast and efficient sensing and removal of sub-nanomolar Hg(II). All results indicated that $2DC_3N_3$ can be used as both a sensor and an adsorbent for the detection and removal of Hg(II) ions in environmental processes. Binding of Hg(II) to $2DC_3N_3$, as evidenced by DFT computational studies, demonstrates a high degree of the material's potential for selective detection. HOMO−LUMO energies and geometric properties, including bond length and angle, showed cooperative interactions between the nitrogen atoms of $2DC_3N_3$ and Hg^{2+}, indicating a high specificity for this platform toward mercury ions. The high sensitivity, significant selectivity, good adsorption capacity, and sub-nanomolar detection limit demonstrated a high potential for $2DC_3N_3$ to monitor and remove Hg(II) from contaminated water. $2DC_3N_3$ was successfully recovered after detecting mercury ions and used for the next run of detection.

EXPERIMENTAL SECTION

Materials and Methods. Additional information regarding synthesis of $2DC_3N_3$, including materials, methods, synthetic protocols as well as characterizations, can be found in the Supporting Information.

Synthesis of $2DC_3N_3$. A mixture of cyanuric chloride (3 g, 16.26 mmol) and sodium cyanide (2.4 g, 3 × 16.26 mmol) was mixed and stirred at 10 °C for 30 min under nitrogen atmosphere. Subsequently, 30 mL of THF was cautiously added to the mixture within 10 min. The reaction mixture was then stirred at 10 °C for 5 h, followed by stirring at 65 °C for 3 days. The mixture was dialyzed using a dialysis bag (2 kDa) against water for 3 days and then methanol for 2 days and finally water for 1 day. Product was lyophilized, and 1.8 g of black solid compound was obtained.

Preparation of Stock Solutions of Metal Ions. The ion stock solutions (1 mM) were prepared by dissolving $SnCl_2$, the corresponding nitrate salts of Ca^{2+}, Cd^{2+}, Co^{2+}, Cr^{2+}, Mg^{2+}, Ni^{2+}, Pb^{2+}, Mn^{2+} and Zn^{2+} as well as acetate salts of Cu^{2+} and Hg^{2+} in ultrapure water and used for further experiments. The stock solution of EDTA (0.15 M) was prepared in ultrapure water. NaOH (1 M) and HCl (1 M) were used to adjust pH.

Fluorescence Sensing Experiments. $2DC_3N_3$ (1.5 mg) was dispersed in ultrapure water (10 mL), followed by sonication for 20 min to ensure a homogeneous mixture, prior to fluorescence measurements. The fluorescence spectra were recorded immediately after an appropriate aliquot of the stock solution (150 μM) of ions was added. The fluorescence emission spectra were recorded at 298 K and repeated three times to get concordant results. The suspensions of $2DC_3N_3$ were excited at a wavelength of 360 nm, and the resulting emission wavelengths were monitored from 370 to 600 nm. The fluorescence titration measurement was recorded after the stock solution (0−300 μM) of Hg^{2+} was added to the $2DC_3N_3$ solution (0.15 mg·mL^{-1}). For the recycling of $2DC_3N_3$, the stock solution of EDTA (0.15 M) was added to remove Hg^{2+} from $2DC_3N_3/Hg^{2+}$, and the recycled $2DC_3N_3$ was reused in the next Hg^{2+} detection test and removal. The fluorescence efficiency was determined using the equation $[(F_0 - F)/F_0 \times 100\%]$, where F_0 represents the initial fluorescence intensity.

Fluorescence Quenching of $2DC_3N_3$ by Hg^{2+}. The possible quenching mechanism can be interpreted using the Stern Volmer equation $F_0/F = 1 + K_{sv}[Q]$, where the F_0 and F are the fluorescence intensities of the $2DC_3N_3$ suspension without and with the addition of Hg^{2+}, respectively, K_{sv} is the Stern−Volmer quenching constant, measuring the efficiency of quenching, and [Q] is the quenching concentration. The binding constant (K) and the number of binding sites (n) between $2DC_3N_3$ and Hg^{2+} have been calculated using eq 1 for the quenching process:

$$\log [(F_0 - F)/F] = \log K + n \log [Q] \quad (1)$$

A plot slope of $\log [(F_0 - F)/F]$ versus $\log [Q]$ is equal to n (the number of binding sites of Hg^{2+} on $2DC_3N_3$) and the intercept on the Y-axis is equal to $\log K$ (K equal to the binding constant).[33,34]

Adsorption of Hg^{2+}. To investigate the capacity of $2DC_3N_3$ for Hg^{2+} adsorption, 1 mg of this platform was incubated with 20 mL of aqueous solution containing 20 mg·L^{-1} of Hg^{2+}. Then concentrations of residual metal ion were assessed by Atomic Absorption Spectroscopy (AAS). All experiments were repeated three times under the same conditions to ensure the reliability and correctness of experimental data. The adsorption capacity of the $2DC_3N_3$ for Hg^{2+} ion was calculated by the following eq 2:

$$q_e = \frac{(C_0 - C_e)V}{m} \quad (2)$$

where q_e (mg·g^{-1}) represents the amount of Hg^{2+} ion adsorbed on the $2DC_3N_3$ at equilibrium and C_0 and C_e (mg·L^{-1}) represent the initial and equilibrium concentrations of Hg^{2+} solution, respectively. Also, V (L) and m (g) are the volume of the Hg^{2+} solution and mass of $2DC_3N_3$, respectively. The Hg^{2+} ion removal efficiency (R, %) was calculated using the following eq 3:[35]

$$R(\%) = \frac{(C_0 - C_e)}{C_0} \times 100 \quad (3)$$

To evaluate the adsorption mechanism of Hg^{2+} ion on the $2DC_3N_3$, the pseudo-first-order and pseudo-second-order kinetic models were employed fitting the experimental data, and the equations could be indicated as (4) and (5), respectively:

https://doi.org/10.1021/acsapm.4c01770
ACS Appl. Polym. Mater. 2024, 6, 11750−11761

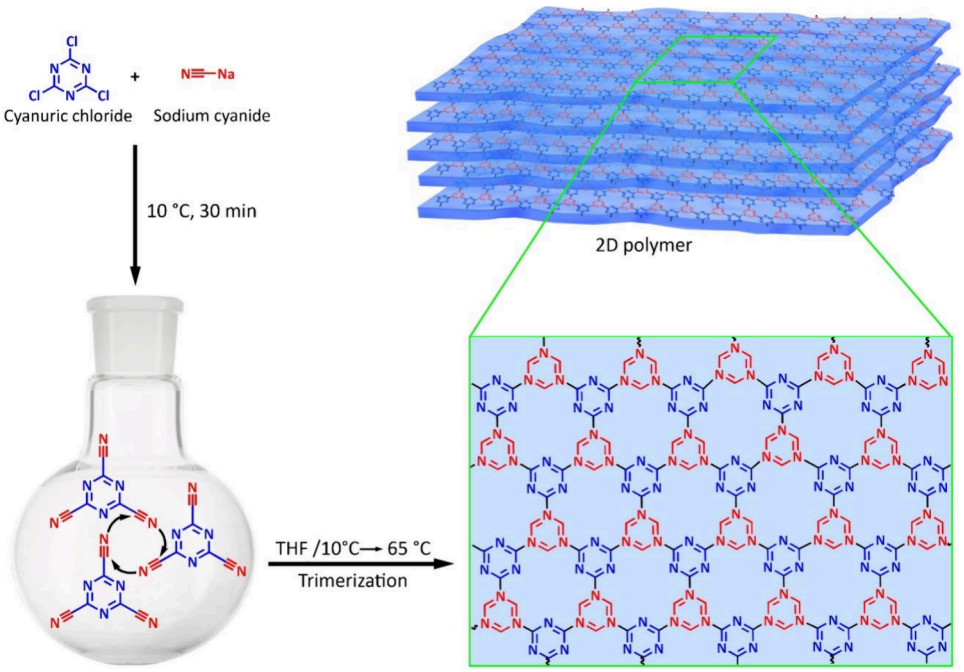

Figure 1. Schematic representation of the synthesis of $2DC_3N_3$. Reaction between cyanuric chloride and sodium cyanide resulted in reactive intermediates that changed to two-dimensional frameworks. Stacking many layers of $2DC_3N_3$ by noncovalent interactions resulted in bigger three-dimensional structures.

$$\ln(q_e - q_t) = \ln q_e - K_1 t \quad (4)$$

$$t/q_t = 1/K_2 q_e^2 + t/q_e \quad (5)$$

where q_e (mg·g^{-1}) is the equilibrium adsorption capacity of Hg^{2+} ion, q_t (mg·g^{-1}) is the amount of the adsorbed Hg^{2+} ion at adsorption time t (min), and k_1 (min^{-1}) and k_2 (g·mg^{-1} min^{-1}) are the rate constants of the pseudo-first-order and the pseudo-second-order reaction, respectively.[36]

Freundlich and Langmuir models were applied to the obtained experimental results to interpret the adsorption mechanism. Equations 6 and 7 indicate the linearized forms of the Langmuir and Freundlich isotherms, respectively:

$$C_e/q_e = 1/K_L Q_m + C_e/Q_m \quad (6)$$

$$\ln q_e = \ln K_F + 1/n \ln C_e \quad (7)$$

where Q_m (mg·g^{-1}) is the maximum adsorption capacity of the Hg^{2+}, C_e (mg·L^{-1}) is the equilibrium concentration of Hg^{2+}, q_e (mg·g^{-1}) is the equilibrium adsorption of Hg^{2+} ion, and K_L (L·g^{-1}), K_F (mg$^{1-1/n}$·L$^{1/n}$·g^{-1}) and $1/n$ are the Langmuir and Freundlich constants and the adsorption intensity of the adsorbent $2DC_3N_3$, respectively.[37]

To investigate the effect of temperature on the adsorption process of Hg^{2+} ion by $2DC_3N_3$ and energy exchange, thermodynamic parameters were calculated using eqs 8, 9 and 10:

$$K_c = q_e/C_e \quad (8)$$

$$\ln K_c = \Delta S^\circ/R - \Delta H^\circ/RT \quad (9)$$

$$\Delta G^\circ = \Delta H^\circ - T\Delta S^\circ \quad (10)$$

where K_c (L·mg^{-1}) is the constant of standard thermodynamic equilibration, q_e (mg·g^{-1}) is the amount of Hg^{2+} ion adsorbed on the $2DC_3N_3$ at equilibrium, C_e (mg·L^{-1}) is the amount of Hg^{2+} in the solution after adsorption, R is the universal gas constant (8.314 J·mol^{-1} K^{-1}) and T (K) is the absolute temperature. ΔG° (J mol^{-1}) is the change in Gibbs free energy, ΔH° (J mol^{-1}) is the change in enthalpy, and ΔS° (J mol^{-1} K^{-1}) is the change in entropy. By van't Hoff linear plotting between ln K_c and $1/T$, the values of ΔH° and ΔS° were obtained from the slope and intercept.[38,39]

Computational Studies. The geometry of molecules was optimized using density functional theory (DFT) in the water phase using the C-PCM method. The obtained structure for $2DC_3N_3$ was also matched with suggested structures in the literature.[40] The optimizations were checked by using vibrational frequency calculations. The heavy metals were adsorbed on the surface of plausible configurations of pristine $2DC_3N_3$ by allowing coordination in the $2DC_3N_3$/M system until minimum energy is realized. From this optimized structure, other theoretical values including HOMO–LUMO energy, total energy, bond angle, and bond length of the target molecules were calculated. In addition, MEP surface maps were determined. The adsorption energy for the stabilization of M on the $2DC_3N_3$ sensor was calculated by[41]

$$DE_{ads} = E_{2DC3N3/M} - (E_M + E_{2DC3N3}) \quad (11)$$

where $2DC_3N_3$/M is the after-adsorption complex, $2DC_3N_3$ is the bare nanosheet, and M is the heavy metal cation. This theory, which contains a hybrid functional within the framework of the cluster modeling approach, has been established as an accurate method for studying the chemistry of complex systems that incorporate metals and main-group elements.[42]

RESULTS AND DISCUSSION

To avoid high temperature carbonization and side reactions, the synthesis of $2DC_3N_3$ was initially performed at 10 °C by catalyst-free [2+2+2] cyclotrimerization of the product of reaction between cyanuric chloride and sodium cyanide followed by stirring at 65 °C. The synthesis route of $2DC_3N_3$ is shown in Figure 1. The structure of $2DC_3N_3$ was characterized by different spectroscopy and microscopy methods, as well as thermal and elemental analysis. In high resolution transmission electron microscopy (HRTEM), $2DC_3N_3$ exhibited crystalline domains attributed to in-plane reflection, surrounded by amorphous regions corresponding to the vertical spacing of stacked sheets (Figure S1a). The electron diffraction (SAED) pattern revealed faint diffraction rings, corresponding to the (002) and (200) planes, together

https://doi.org/10.1021/acsapm.4c01770
ACS Appl. Polym. Mater. 2024, 6, 11750−11761

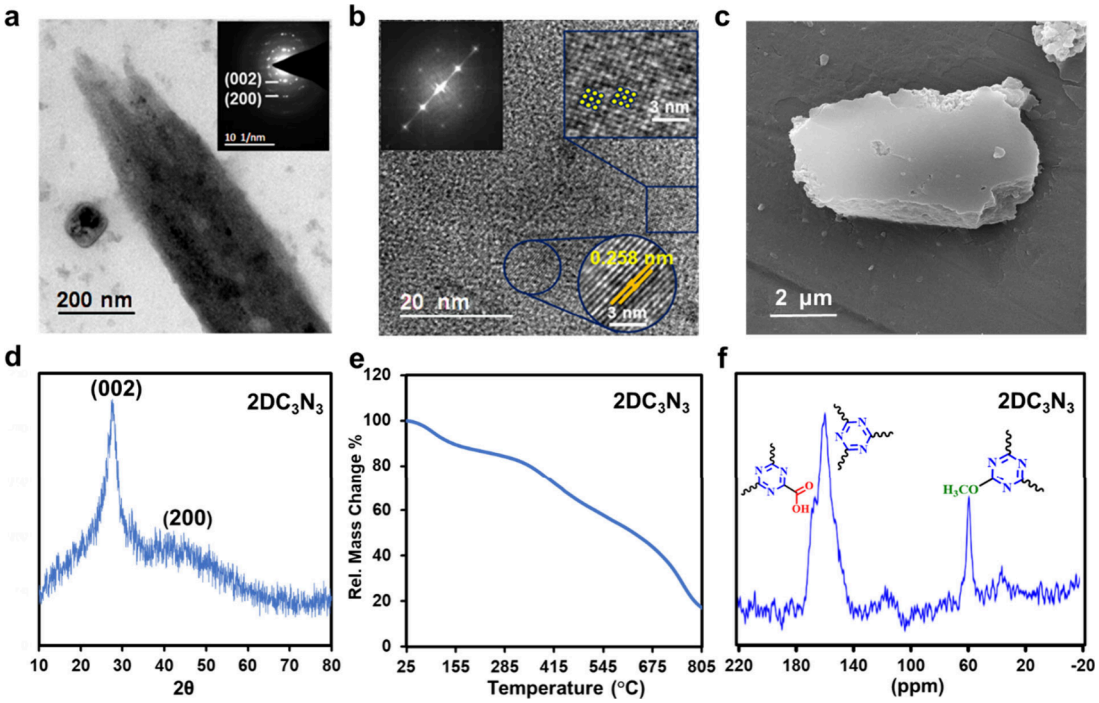

Figure 2. (a) TEM image of a small domain of $2DC_3N_3$ sheets that are stacked as a thick layer. In this image, the inset shows the electron diffraction pattern of the same domain. (b) HRTEM of a $2DC_3N_3$ sheet. In this image, the top right inset shows the unit cell of this compound. Also, the top left inset represents the electron diffraction pattern of the crystalline domain of the sheet, and the bottom right inset shows the 0.258 nm interlayer distance for the stacked layers. (c) SEM image of $2DC_3N_3$ sheets. (d) XRD diffractograms of $2DC_3N_3$. (e) TGA thermograms of $2DC_3N_3$ at a heating rate of 10 °C. min^{-1} under argon. (f) CP-MAS NMR spectrum of $2DC_3N_3$, showing distinguished signals for the triazine rings, methoxy, and carboxyl functional groups.

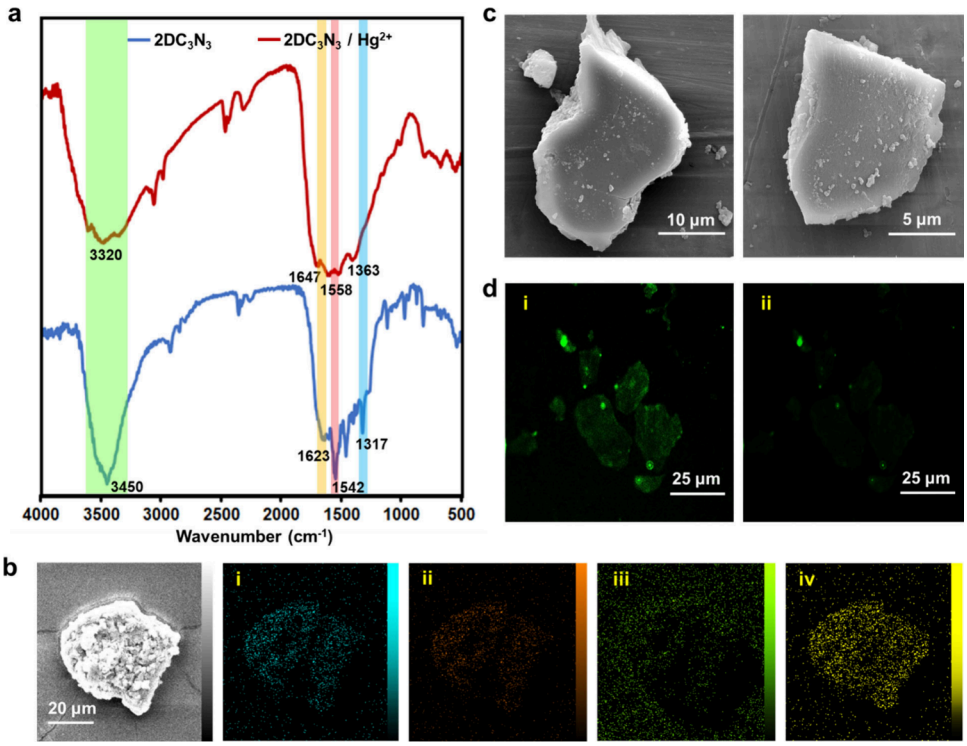

Figure 3. (a) IR spectra of $2DC_3N_3$ before and after the addition of Hg^{2+}. (b) Elemental maps of $2DC_3N_3/Hg^{2+}$ representing homogeneous scattering of carbon (i), nitrogen (ii), oxygen (iii) and mercury (iv) elements in this complex. (c) SEM images of $2DC_3N_3/Hg^{2+}$ sheets. (d) Confocal laser scanning microscopy (CLSM) image of $2DC_3N_3$ sheets exited at 405 nm before (i) and after addition of Hg^{2+} (ii).

with a sharp peak at 2θ 27° accompanied by broad shoulders centered at 2θ 41° in the X-ray diffractogram of this compound (Figure 2a, d).[26,43] The distance between stacked layers of $2DC_3N_3$ was 0.258 nm, in agreement with the value obtained

https://doi.org/10.1021/acsapm.4c01770
ACS Appl. Polym. Mater. 2024, 6, 11750−11761

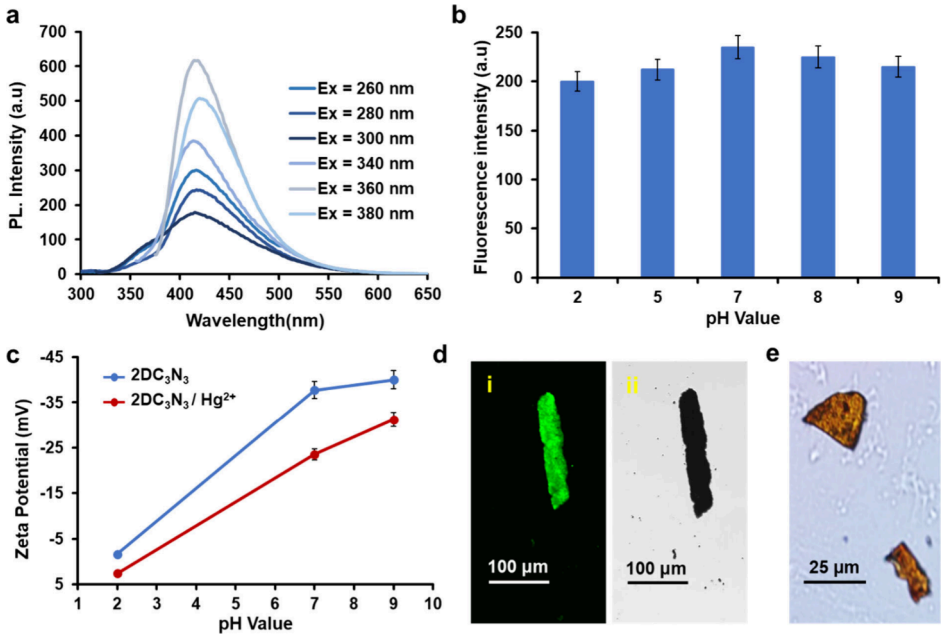

Figure 4. (a) The photoluminescence (PL) spectra of $2DC_3N_3$ (0.5 mg.mL^{-1}) in aqueous solution exited at different wavelengths. (b) Intensity of the photoluminescence of $2DC_3N_3$, excited at 360 nm, upon changing pH values. (c) Zeta potential values of $2DC_3N_3$ (1 mg.mL^{-1}) before and after addition of 150 μM Hg^{2+} ion versus pH, indicating dependence of surface charge of this platform on pH. (d) Confocal laser scanning microscopy image (i) of $2DC_3N_3$ exited at 405 nm. Figure (ii) shows the bright field image of the same sheet shown in Figure (i). (e) Optical microscopy images of $2DC_3N_3$ sheets.

from XRD and electron diffraction pattern measurements (Figure 2b, Figure S1b).[44] AFM images revealed typical morphologies, such as back-folding in $2DC_3N_3$ with several micrometers lateral size and clear edges (Figure S1c).[45] The cryo-TEM image of $2DC_3N_3$ displayed the covalent nature of the two-dimensional structures with several micrometers lateral size and high transparency, indicating monolayers or few layers (Figure S1d). Moreover, in agreement with the HRTEM and conventional TEM images, scanning electron microscopy (SEM) showed a sheet-like flat morphology with several micrometers lateral size for $2DC_3N_3$ (Figure 2c, Figure S2a). In the SEM images, layers of $2DC_3N_3$ that are stacked can be clearly seen. The composition of the synthesized $2DC_3N_3$ was investigated by elemental analysis (EA) and energy dispersive X-ray spectroscopy (EDX) elemental mapping. The carbon/nitrogen (C/N) ratios of $2DC_3N_3$ measured by EDX and elemental analysis were 1.08 and 1.03 (Figure S3a). Also, carbon, nitrogen, and oxygen element scattering patterns indicated an integrated structure for $2DC_3N_3$ (Figures S3b and S4a). The TGA thermogram of $2DC_3N_3$ resembled the reported data for similar triazine frameworks,[46,47] with three main weight losses occurring at 100−150 °C, 350−550 °C, and 650−800 °C, corresponding to the evaporation of surface moisture, detachment of functional groups, and decomposition of the backbone, respectively (Figure 2e). In the ^{13}C solid-state cross-polarization magic-angle-spinning (CP-MAS) nuclear magnetic resonance (NMR) spectra, the signal at 160 ppm was assigned to carbon atoms of triazine rings (Figure 2f). Furthermore, a signal at 55 ppm and a shoulder at 170 ppm confirm the methoxy and carbonyl groups at the edge of $2DC_3N_3$ sheets, respectively. The absence of aliphatic and other aromatic carbons indicated minimized side reactions and a well-defined structure.[48]

The structure of $2DC_3N_3$ and inclusion of Hg^{2+} ions into the pores of this compound was investigated by IR, SEM, EDX and confocal laser scanning microscopy (CLSM). In IR spectra, the presence of a C=N absorbance band at 1542 and 1317 cm^{-1} and the absence of a C≡N bond at 2200 cm^{-1} indicated the production of an integrated structure consisting of triazine rings. Also, a strong absorbance band at 1623 cm^{-1} and a broad absorbance band at 3000−3600 cm^{-1} were assigned to the carboxyl functional groups at the edge of $2DC_3N_3$. Interactions between Hg^{2+} and $2DC_3N_3$ were verified by comparison IR spectra of $2DC_3N_3$ in the presence and absence of metal ions (Figure 3a).[49] Upon addition of Hg^{2+} ions, the absorbance bands of $2DC_3N_3$ were broadened and significantly shifted, suggesting the interactions between triazine rings and Hg^{2+}.[50] Moreover, elemental mapping and SEM images showed a high amount of Hg^{2+} ions trapped on the surface of $2DC_3N_3$ (Figure 3b, c, Figures S2b, S3a, and S4b).[51] The fluorescence of $2DC_3N_3$ sheets was dramatically quenched after incubation with Hg^{2+} ions (Figure 3d).[52,53] These results indicated that $2DC_3N_3$ is highly efficient to adsorb Hg^{2+} ions.

To explore the fluorescence property of $2DC_3N_3$, the effects of the excitation wavelength and pH on the fluorescence intensity of this framework were investigated by photoluminescence (PL) spectroscopy. $2DC_3N_3$ sheets dispersed in H_2O (0.5 mg·mL^{-1}) were exited at 360 and 380 nm and emitted strong luminescence at 415 and 420 nm with 63% quantum yield, which is much higher than that for other similar materials (Figure 4a).[54] Moreover, the fluorescence intensity of $2DC_3N_3$ did not change in a broad range of pH values significantly, indicating the stability of this platform in different mediums (Figure 4b). Also, this result showed that the PL of $2DC_3N_3$ was mainly due to its π-conjugated system and independent from its oxygen containing functional groups. In spite of this PL, the surface charges of $2DC_3N_3$ and $2DC_3N_3/Hg^{2+}$ were changed dramatically by pH variation. This behavior indicated that the surface charges of $2DC_3N_3$ and $2DC_3N_3/Hg^{2+}$ with increase in H^+ and OH^- ions at different

https://doi.org/10.1021/acsapm.4c01770
ACS Appl. Polym. Mater. 2024, 6, 11750−11761

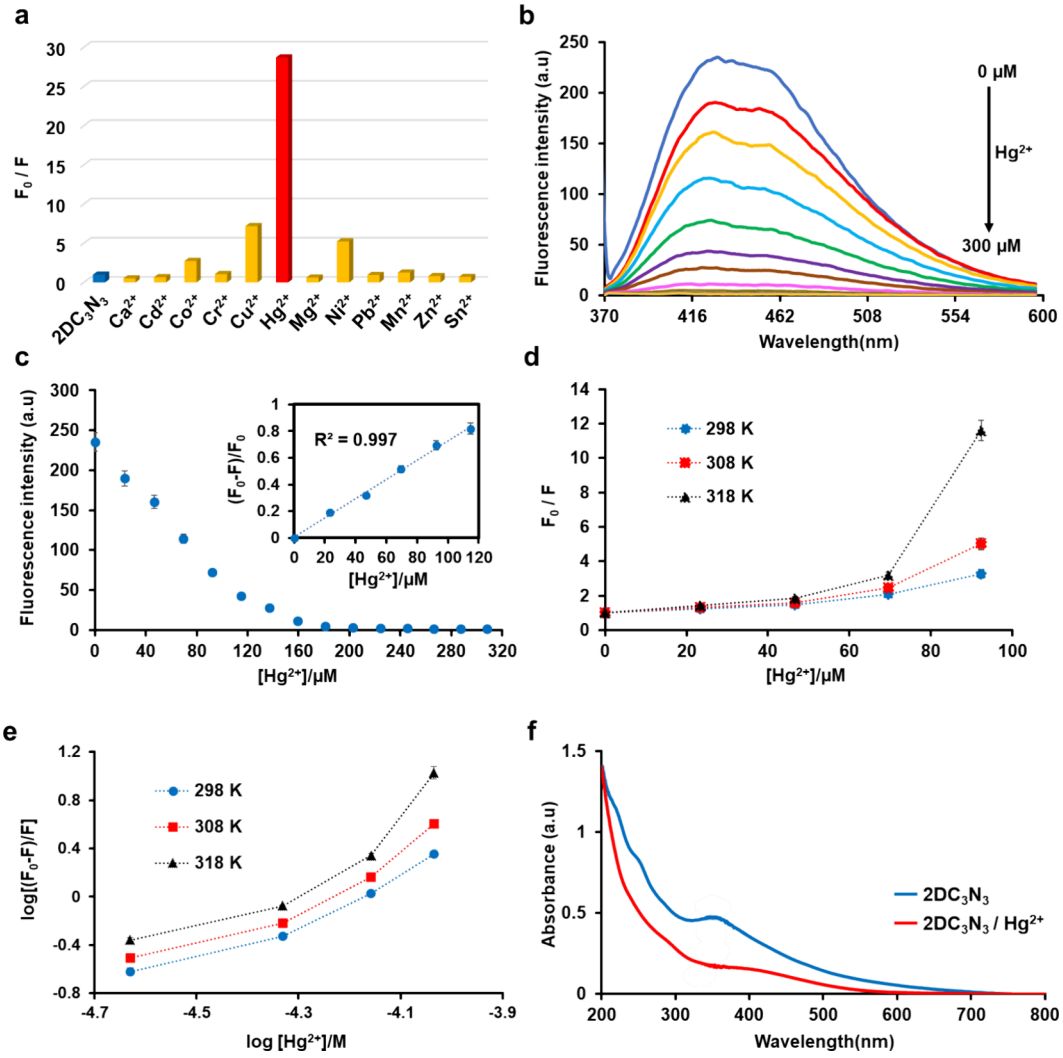

Figure 5. (a) The fluorescence intensity of aqueous solution of $2DC_3N_3$ (0.15 mg.mL^{-1}), excited at 360 nm excitation wavelength in the presence of 150 μM of various metal ions. (b) The fluorescence emission spectra of $2DC_3N_3$ upon gradual addition of Hg^{2+} (λ_{ex} = 360 nm). (c) The fluorescence intensity of aqueous solution of $2DC_3N_3$ (0.15 mg.mL^{-1}), excited at 360 nm, vs the concentration of Hg^{2+}. (Inset: The linear calibration plot for Hg^{2+} detection.) (d) Stern−Volmer plots of $2DC_3N_3$ in the presence of Hg^{2+} at different temperature (λ_{ex} = 360 nm). (e) Plots of the Hg^{2+} quenching effect on $2DC_3N_3$ fluorescence at different temperature. (f) UV−vis absorption spectra of $2DC_3N_3$ (0.15 mg.mL^{-1}) before and after addition of 150 μM Hg^{2+} ion.

pHs were dominated by their oxygen containing functional groups (Figure 4c). In order to gain more information about the PL of $2DC_3N_3$, confocal laser scanning microscopy (CLSM) images of individual sheets were recorded and revealed a strong emission for the whole backbone of $2DC_3N_3$ sheets upon excitation by a suitable wavelength (Figure 4d, e).

Because of the high toxicity of most metal ions, design and synthesis of new materials for the selective and efficient sensing of these ions in aqueous solution is of high importance. The synthesized $2DC_3N_3$ containing triazine rings with six lone-pair electrons and high negative surface charge meets requirements for the construction of a fluorescent sensor to detect heavy metal cations. One of the mechanisms, through which $2DC_3N_3$ will be able to sense such metal ions, is electron transfer from the excited sheets to the partially filled d-orbitals of the metal cations so-called photoinduced electron transfer (PET) pathway.[55] To evaluate the selectivity of $2DC_3N_3$ as a sensing system, an aqueous solution (150 μM) of various biologically and environmentally relevant metal ions including Ca(II), Cd(II), Co(II), Cr(II), Cu(II), Mg(II), Ni(II), Pb(II), Mn(II), Zn(II), Sn(II) and Hg(II) wan added to an aqueous solution of $2DC_3N_3$ (0.15 mg.mL^{-1}) and the fluorescent spectra of sheets were recorded. As shown in Figure 5a, the fluorescence of $2DC_3N_3$ was effectively quenched by Hg^{2+} ions, while it did not change significantly in the presence of other metal ions. Strong fluorescence quenching (96.52%) indicated a high selectivity for $2DC_3N_3$ toward Hg^{2+}.

To explore the sensitivity of $2DC_3N_3$ to Hg^{2+}, the fluorescence of this platform was recorded in the presence of different concentrations of Hg^{2+}. Figure 5b shows the fluorescence intensity of $2DC_3N_3$ versus the Hg^{2+} concentration (0 μM to 300 μM). The fluorescence intensity of $2DC_3N_3$ at around 428 nm decreased gradually with increasing Hg^{2+} concentration and was almost completely quenched by the addition of 160 μM of Hg^{2+}. A good linear correlation (R^2 = 0.997) in Figure 5c at low concentrations from 0 to 115 μM was observed. The limit of detection (LOD) of $2DC_3N_3$ for mercury ions was estimated to be 0.98 nM, that is much lower than previously reported fluorescent sensors.[56,57] To investigate the mechanism, the fluorescence quenching process was

https://doi.org/10.1021/acsapm.4c01770
ACS Appl. Polym. Mater. 2024, 6, 11750−11761

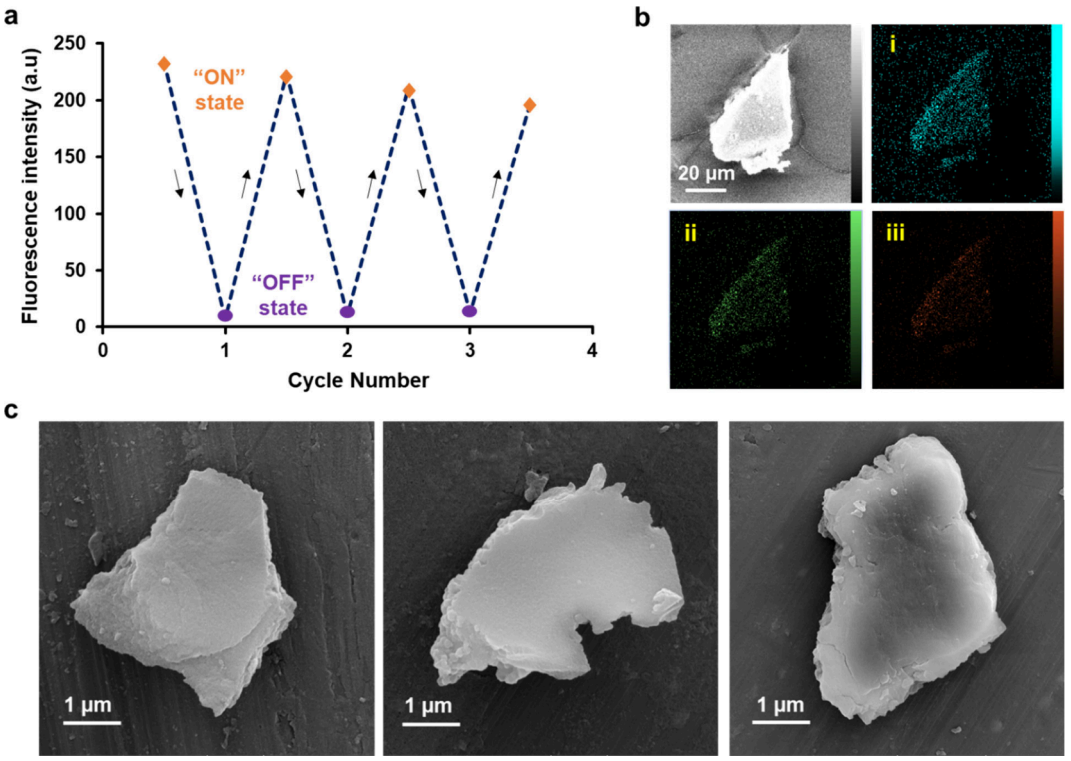

Figure 6. (a) Recyclability of $2DC_3N_3$ for sensing Hg^{2+}. $2DC_3N_3$ was incubated with Hg^{2+} ions and then mixed with EDTA to remove the adsorbed ions. In these cycles, fluorescence of $2DC_3N_3$ sheets was on and off upon incubation with Hg^{2+} and EDTA, respectively. (b) Elemental mapping of $2DC_3N_3$ indicating the successful removal of Hg^{2+} from $2DC_3N_3$. Only carbon (i), nitrogen (ii), and oxygen (iii) elements were detected for $2DC_3N_3$. (c) SEM images of $2DC_3N_3$ sheets from left to right in three different runs of sensing and recycling. After sensing Hg^{2+}, $2DC_3N_3$ were recycled by EDTA solutions (0.15 M).

analyzed using Stern−Volmer and modified Stern−Volmer plots as plots of F_0/F versus $[Q]$ and log $[(F_0 - F)/F]$ versus log $[Q]$ in the range 298 to 318 K, and quenching parameters are reported in Table S1. As shown in Figure 5d, the Stern−Volmer plot deviated from linearity toward the y-axis from the concentration 70 μM Hg^{2+}, and this indicates that quenching is partly static (ground state complex formation) in nature. The values of K_{sv} and K increase with increasing temperature, thus implying that the process may be partly dynamic (collisional interaction). The binding stoichiometries were approximately equal to one, where there must be a single binding site in $2DC_3N_3$ for Hg^{2+} (Figure 5e and Table S1). Considering the K_{sv} and the binding parameters such as the number of sites and the binding constants, the steady-state fluorescence method exhibits a strong binding between $2DC_3N_3$ and Hg^{2+}. Therefore, from Stern−Volmer plots it is confirmed that $2DC_3N_3$ is quenched by mixed static and dynamic quenching mechanisms.[55,58,59] In addition to fluorescence quenching, the effect of the Hg(II) ion on the UV absorption of $2DC_3N_3$ was also studied. Figure 5f shows the UV−vis spectra of $2DC_3N_3$ before and after addition of Hg^{2+}. A broad absorption band from 220 to 600 nm with a band gap of 2.83 eV was assigned to the huge π conjugated system of $2DC_3N_3$ (Figure S4d).[60] Upon addition of 150 μM Hg^{2+}, the UV−vis absorption of $2DC_3N_3$ changed significantly and the absorptions at 220 and 250 nm disappeared, and the absorption at 350 nm became weaker.

Recyclability is a cost-effective and crucial factor in designing novel materials and devices, improving their sustainability and decreasing their negative environmental impacts.[61] The recovery of $2DC_3N_3$ was investigated by adding ethylenediaminetetraacetic acid (EDTA) solution (0.15 M), as a strong chelating agent, to the $2DC_3N_3/Hg^{2+}$ solution and then washing for three consecutive cycles (Figure 6a).[62,63] According to Pearson's HSAB principle, the Hg^{2+} ion is a soft acid and nitrogen is a hard base, leading to weak interactions between them.[64] Such interactions change the PL of $2DC_3N_3$ dramatically but can be disturbed by stronger ligands such as EDTA. Energy dispersive X-ray spectroscopy (EDX) elemental mapping and SEM images showed that Hg^{2+} ions are removed from $2DC_3N_3$ by addition of EDTA but the structure of sheets is well preserved after recycling (Figure 6b, c, Figures S3a and S4c). The fluorescence intensity of $2DC_3N_3$ in three cycles did not change significantly, indicating recyclability of this platform and its reusability to detect Hg^{2+}.

The accumulation of metal ions in drinking water has become a serious problem for public health. Detection of these environmental pollutants through fluorescent sensors has gained widespread attention because of their high sensitivity, good selectivity, low cost, simple operation, and high accuracy. Therefore, development of platforms and sensors for removal and detection of metal cations, especially mercury ion, is important, as it causes serious health and negative environment impacts.[65,66]

$2DC_3N_3$, with a large number of heteroatoms, high surface area, stability, and negative surface charge, is an excellent candidate for sensing and removing Hg^{2+} from aqueous solutions. As shown in Figure 5a, $2DC_3N_3$ showed the highest selectivity toward Hg^{2+} ions in comparison with other metal ions. The pore properties of $2DC_3N_3/Hg^{2+}$ were evaluated by using BET nitrogen the adsorption−desorption isotherm and the corresponding BJH pore size distribution curves at 77 K,

https://doi.org/10.1021/acsapm.4c01770
ACS Appl. Polym. Mater. 2024, 6, 11750−11761

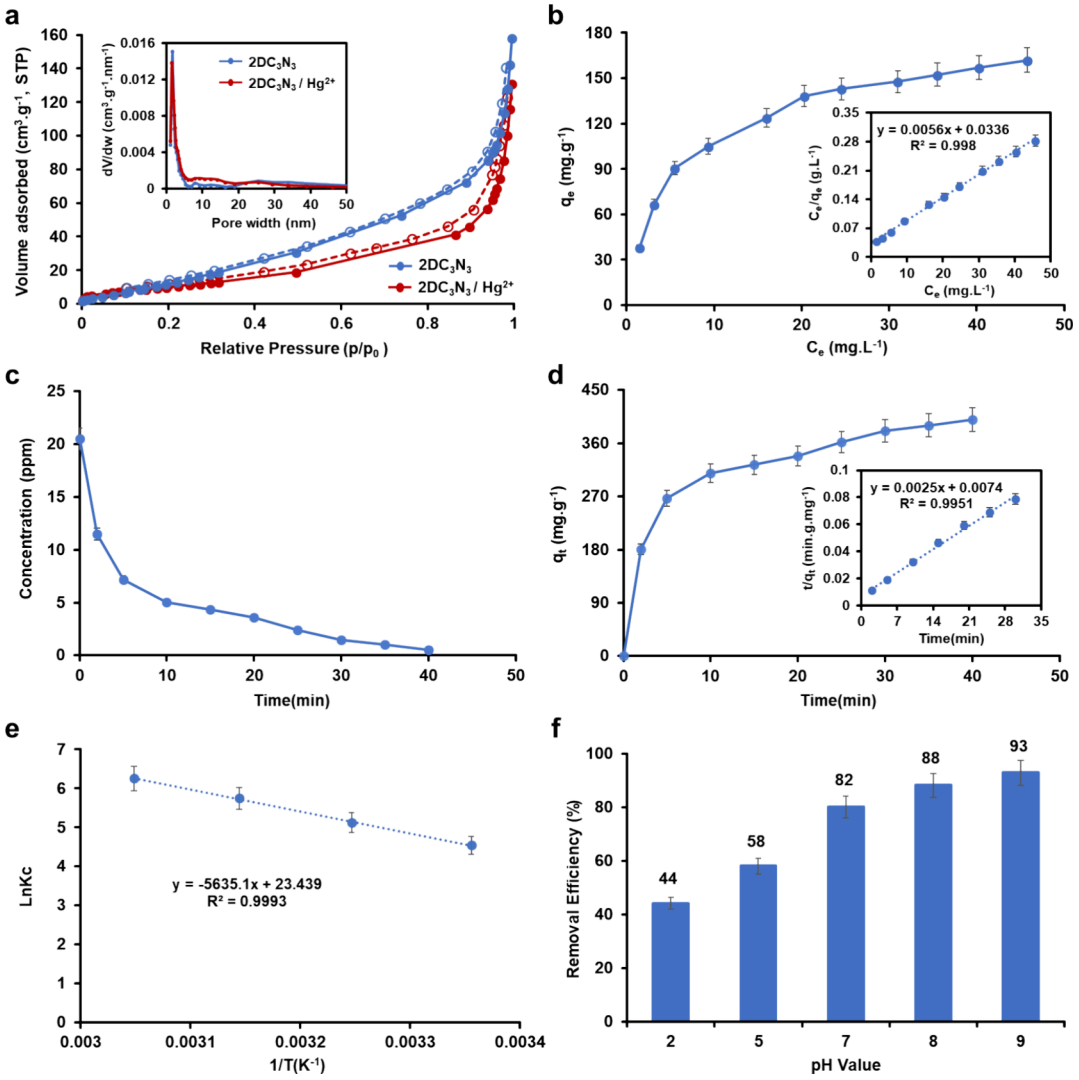

Figure 7. (a) Nitrogen adsorption−desorption isotherms of $2DC_3N_3$ and $2DC_3N_3/Hg^{2+}$ at 77 K. Inset shows pore size distribution (PSD) curve of $2DC_3N_3$ and $2DC_3N_3/Hg^{2+}$. (b) Adsorption isotherm of Hg^{2+} by $2DC_3N_3$. Inset shows the linear regression by fitting the equilibrium adsorption data with the Langmuir adsorption model. (c) Adsorption kinetics of Hg^{2+} on $2DC_3N_3$ (the initial concentration of Hg^{2+} was 20 mg·L^{-1}). (d) Effect of contact time on the adsorption capacity of Hg^{2+} by $2DC_3N_3$. Inset shows the pseudo-second-order kinetic plot for the adsorption of Hg^{2+} (20 mg·L^{-1}). (e) The Van't Hoff plot for the adsorption of Hg^{2+} on $2DC_3N_3$ at different temperature. (f) Removal efficiency of Hg^{2+} at different pH conditions.

which showed the reduction of gas upload. The immobilization of Hg^{2+} on the surface of the polymer resulted in a slight decrease in specific surface area and pore volume to 16 $m^2 \cdot g^{-1}$ and 0.048 $cm^3 \cdot g^{-1}$, respectively. In contrast, 19 $m^2 \cdot g^{-1}$ and 0.052 $cm^3 \cdot g^{-1}$ were determined for $2DC_3N_3$. The average pore diameters of 9.85 and 9.12 nm were obtained for $2DC_3N_3$ and $2DC_3N_3/Hg^{2+}$, respectively, which belong to a type III isotherm according to IUPAC classification (Figure 7a).[24]

Due to such selectivity, adsorption isotherms, adsorption kinetics, and the effect of pH and temperature on the ability of $2DC_3N_3$ to sense and adsorb Hg^{2+} were investigated. $2DC_3N_3$ (1 mg) was added to 20 mL of Hg^{2+} with different concentrations at pH 7.0, and different parameters related to removal of mercury ions were investigated. As shown in Figure 7b and Table S2, the adsorption isotherms of $2DC_3N_3$ for Hg^{2+} are consistent with the Langmuir isotherm model. The saturated adsorption capacity of $2DC_3N_3$ for Hg^{2+} was 178 mg·g^{-1}, indicating excellent affinity of this platform for Hg^{2+}. This is the highest sensitivity and adsorption among previously reported N-rich functional materials.[67] The Hg^{2+} contents of $2DC_3N_3/Hg^{2+}$ were calculated based on the inductively coupled plasma optical emission spectroscopy (ICP-OES) results. It was found that 86% of nitrogen atoms in the structure of $2DC_3N_3$ were used to remove Hg^{2+}. This maximum adsorption capacity for Hg^{2+} can be attributed to the synergistic effect of the well-distributed and accessible nitrogen atoms in the structure of $2DC_3N_3$.

To understand the mechanism of adsorption of Hg^{2+} ions by $2DC_3N_3$, pseudo-first-order and pseudo-second-order kinetic models were investigated for this system.[68,69] As shown in Figure 7c, fast adsorption kinetics was observed in the initial 10 min (>75%) and reached equilibrium within 20 min. Adsorption kinetics was fitted well with the pseudo-second-order model, indicating a porous structure for $2DC_3N_3$ and electrostatic interactions between Hg^{2+} ions and the platform (Figure 7d and Table S3). The increasing value of $\Delta H°$ (46.85 KJ mol^{-1}), the positive value of $\Delta S°$ (194.87 J·mol^{-1} K^{-1}) and the negative values of $\Delta G°$ for $2DC_3N_3$ with increasing

https://doi.org/10.1021/acsapm.4c01770
ACS Appl. Polym. Mater. 2024, 6, 11750−11761

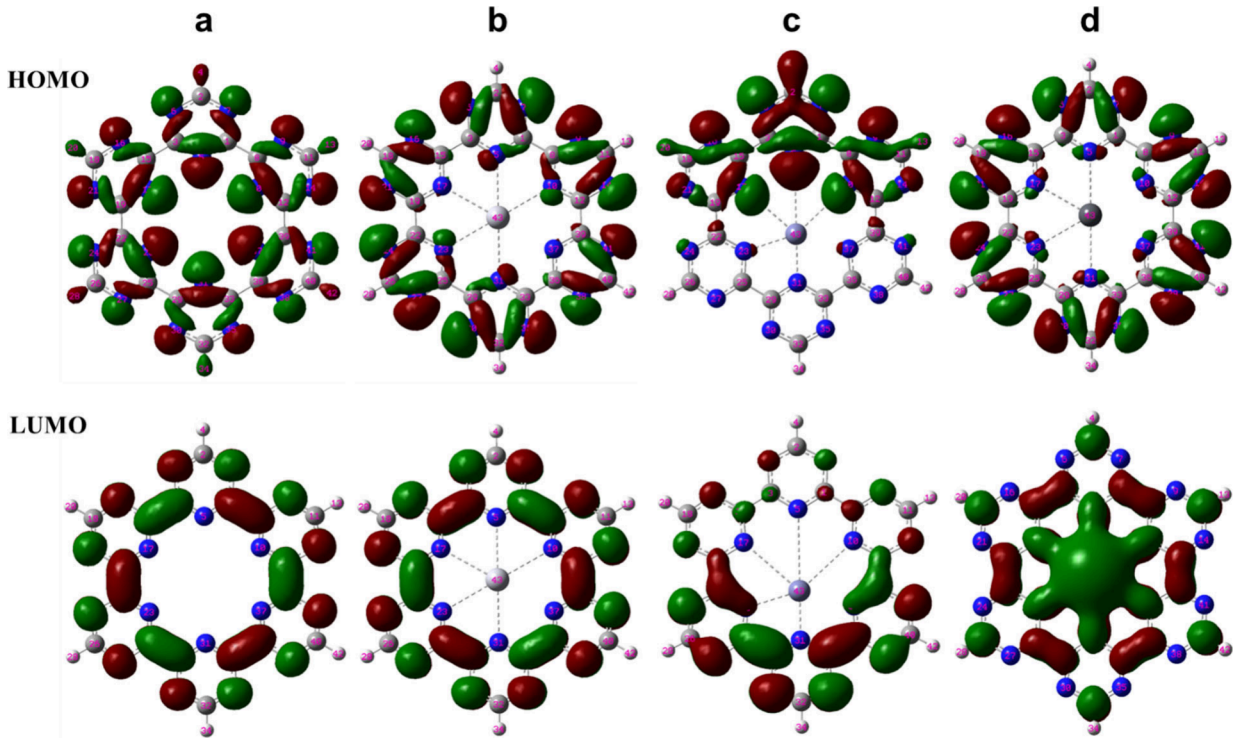

Figure 8. Representation of HOMO and LUMO orbitals for the optimized structures of $2DC_3N_3$ (a), $2DC_3N_3/Hg^{2+}$ (b), $2DC_3N_3/Zn^{2+}$ (c) and $2DC_3N_3/Pb^{2+}$ (d) in the ground state calculated at B3LYP levels. The green and red colors indicate positive and negative phases, respectively.

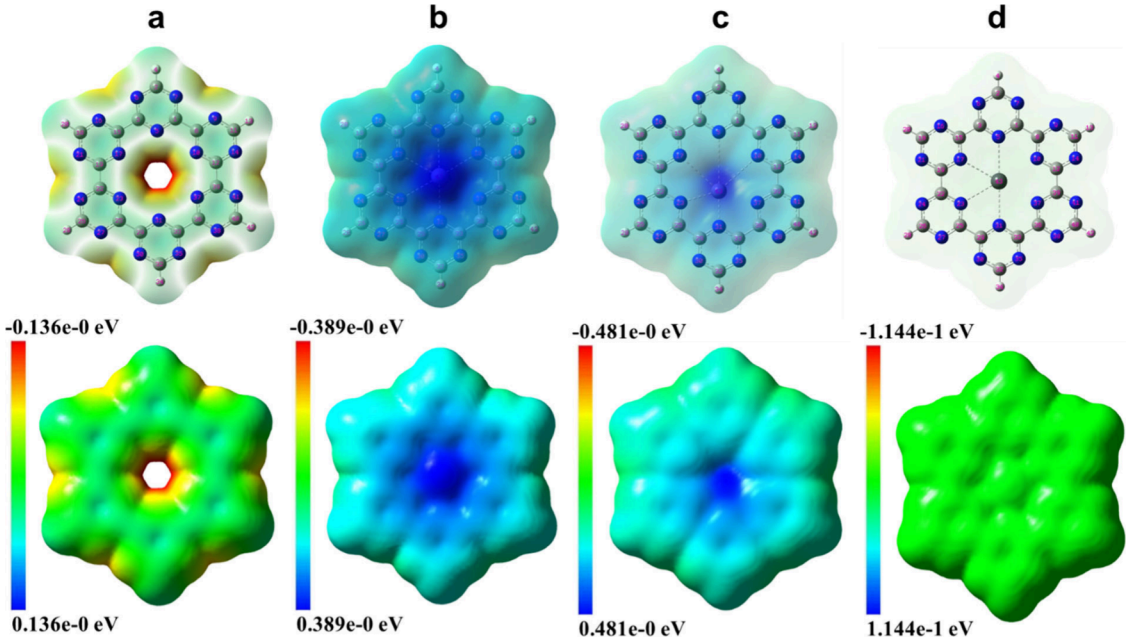

Figure 9. Representation of the MEP for the optimized structures of $2DC_3N_3$ (a), $2DC_3N_3/Hg^{2+}$ (b), $2DC_3N_3/Zn^{2+}$ (c) and $2DC_3N_3/Pb^{2+}$ (d) in the ground state calculated at B3LYP levels.

temperature (298−328 K) at 20 min indicated that due to an increase entropy and mobility of Hg^{2+} ions and interaction with active sites on the surface of $2DC_3N_3$, the adsorption process was endothermic and spontaneously and thermodynamically favorable (Figure 7e and Table S4). For practical applications, the pH value of the solution plays an important role in the mechanism of adsorption. Accordingly, the capacity of $2DC_3N_3$ to adsorb Hg^{2+} ions at different pHs was investigated. $2DC_3N_3$ showed excellent adsorption efficiency (>93%) in alkaline conditions, due to its high negative surface charge (Figure 7f).

In order to gain more information about interactions between metal ions and $2DC_3N_3$, the molecular structures of $2DC_3N_3$, $2DC_3N_3/Hg^{2+}$, $2DC_3N_3/Zn^{2+}$ and $2DC_3N_3/Pb^{2+}$ were optimized using Gaussian software, using the B3LYP functional in the DFT method with the 3-21G(d, p) basis set in the water phase. Relaxation of metal ions interacting with different sites of such platforms has indicated that nitrogen

https://doi.org/10.1021/acsapm.4c01770
ACS Appl. Polym. Mater. 2024, 6, 11750−11761

atoms inside pores are the most favorable sites for complexation.[70] The optimized geometries using vibrational frequency analysis are shown in Figure S5. The ground state geometry optimization was performed for small sheets of $2DC_3N_3$ (Figure S5a). While Hg^{2+} and Zn^{2+} ions were coordinated to five nitrogen atoms of the triazine rings (Figure S5b, S5c), Pb^{2+} interacted with four atoms (Figure S5d).

The geometrical properties (bond length and angle) in Table S5 and Table S6 showed that the Hg−N, Zn−N and Pb−N distances were on average 2.74 2.89, and 2.75 Å. As a result, the Hg^{2+} ions were localized closer to the surface of platforms, due to desirable interactions with the nitrogen atoms indicated by the smaller values of θ (N−Hg−N) (59.53−60.80°) compared to those of the Zn^{2+} and Pb^{2+} ions. The highest occupied molecular orbital (HOMO) and the lowest unoccupied molecular orbital (LUMO) of the optimized geometries are illustrated in Figure 8 and Table S7. The LUMO energy levels decreased in the order of $2DC_3N_3/Hg^{2+}$ < $2DC_3N_3/Zn^{2+}$ < $2DC_3N_3/Pb^{2+}$, all being much lower than that for the original bare platform. The lower energy level of $2DC_3N_3/Hg^{2+}$ can change the emission pathway of exited electrons and results in strong quenching. Moreover, the electron density was distributed symmetrically in the whole structure of sheets in the case of $2DC_3N_3$ and $2DC_3N_3/Hg^{2+}$, while it was localized unsymmetrically for $2DC_3N_3/Zn^{2+}$ and $2DC_3N_3/Pb^{2+}$. The symmetric distribution of electron density can improve cooperative interactions between the nitrogen atoms of the platform and Hg(II).

Molecular electrostatic surface potential (MESP) maps were determined for $2DC_3N_3$, $2DC_3N_3/Hg^{2+}$, $2DC_3N_3/Zn^{2+}$ and $2DC_3N_3/Pb^{2+}$ (Figure 9). Different values of the electrostatic energy are indicated by different colors. The red regions have a negative electrostatic potential, suggesting that they are more likely to donate electrons or are more nucleophilic than the other regions. The blue regions have a positive electrostatic potential with an electrophilic character. After interaction of the platform with metal cations, the positive charge was centralized in the pore of the structure, where there is a high density of nitrogen atoms and negative electrostatic potential. The density and symmetricity of positive charge for $2DC_3N_3/Hg^{2+}$ was more than for other cases, suggesting more efficient interactions between central nitrogen atoms of platform and Hg(II). This improves the specificity of $2DC_3N_3$ toward mercury ions.

CONCLUSION

In this work, highly photoluminescent N-rich two-dimensional triazine frameworks were synthesized by a one-pot catalyst-free [2+2+2] cyclotrimerization of carbonitrile functional groups conjugated to a triazine ring at mild conditions with a quantum yield of 63%. The removal efficiency and detection limit of $2DC_3N_3$ for Hg^{2+} ions were 97% and 0.98 nM, respectively, suggesting this platform as a specific sensor to detect this metal ion in water. This sensor was recyclable, and simulation studies revealed a key role for the nitrogen atoms in the center of pores of the platform for such specific interactions. Our investigations showed a potential for such a platform to detect Hg(II) at sub-nanomolar concentration. Manipulation of the structure and functional groups of such a platform can open a new avenue for exploring new sensors for other water pollutants.

ASSOCIATED CONTENT

Supporting Information

The Supporting Information is available free of charge at https://pubs.acs.org/doi/10.1021/acsapm.4c01770.

Materials and methods, HRTEM, AFM, SEM and Cryo-TEM images of $2DC_3N_3$, Comparative table of $2DC_3N_3$ by EDX and elemental analysis, Mapping of $2DC_3N_3$, Calculated band gap of $2DC_3N_3$, Optimized geometries, Adsorption isotherms and kinetic parameters table, Thermodynamic and binding parameters table, Selected interatomic distances (Å), selected interbond angles (in degrees) and calculated HOMO and LUMO energies for the optimized structures. (PDF)

AUTHOR INFORMATION

Corresponding Author

Mohsen Adeli − *Department of Organic Chemistry, Faculty of Chemistry, Lorestan University, Khorramabad 68141-54316, Iran;* orcid.org/0000-0001-6895-8491; Email: adeli.m@lu.ac.ir, m.aadeli@fu-berlin.de

Authors

Maryam Salahvarzi − *Department of Organic Chemistry, Faculty of Chemistry, Lorestan University, Khorramabad 68141-54316, Iran*

Ebrahim Mehdipour − *Department of Organic Chemistry, Faculty of Chemistry, Lorestan University, Khorramabad 68141-54316, Iran*

Mohammad Nemati − *Department of Organic Chemistry, Faculty of Chemistry, Lorestan University, Khorramabad 68141-54316, Iran*

Complete contact information is available at: https://pubs.acs.org/10.1021/acsapm.4c01770

Notes

The authors declare no competing financial interest.

ACKNOWLEDGMENTS

We would like to thank Iran Science Elites Federation and Iran National Science Foundation (Project Number 4001281) for the financial support.

REFERENCES

(1) Gomez-Suarez, M.; Chen, Y.; Zhang, J. Porous organic polymers as a promising platform for efficient capture of heavy metal pollutants in wastewater. *Polym. Chem.* **2023**, *14* (35), 4000−4032.

(2) Waqas, W.; Yuan, Y.; Ali, S.; Zhang, M.; Shafiq, M.; Ali, W.; Chen, Y.; Xiang, Z.; Chen, R.; Ikhwanuddin, M. Toxic effects of heavy metals on crustaceans and associated health risks in humans: a review. *Environmental Chemistry Letters* **2024**, *22*, 1391−1411.

(3) Ayodhya, D. Recent progress on detection of bivalent, trivalent, and hexavalent toxic heavy metal ions in water using metallic nanoparticles: A review. *Results in Chemistry* **2023**, *5*, 100874.

(4) Wu, B.; Ga, L.; Wang, Y.; Ai, J. Recent Advances in the Application of Bionanosensors for the Analysis of Heavy Metals in Aquatic Environments. *Molecules* **2024**, *29* (1), 34.

(5) Amalraj, A.; Pavadai, R.; Subramanian, S.; Perumal, P. Fabrication of multi-functional CuO@ PDA-MoS2 mediated dual-functional fluorescence Aptamer for the detection of Hg2+ ions and chloramphenicol through desulfurization cleavage reaction and exonuclease I activity. *Appl. Surf. Sci.* **2022**, *602*, 154222.

(6) Singh, V.; Mishra, A. K. Green and cost-effective fluorescent carbon nanoparticles for the selective and sensitive detection of iron

(III) ions in aqueous solution: mechanistic insights and cell line imaging studies. *Sens. Actuators, B* **2016**, *227*, 467−474.
(7) Li, M.; Shi, Q.; Song, N.; Xiao, Y.; Wang, L.; Chen, Z.; James, T. D. Current trends in the detection and removal of heavy metal ions using functional materials. *Chem. Soc. Rev.* **2023**, *52*, 5827−5860.
(8) Fei, Y.; Hu, Y. H. Design, synthesis, and performance of adsorbents for heavy metal removal from wastewater: a review. *Journal of Materials Chemistry A* **2022**, *10* (3), 1047−1085.
(9) Amalraj, A.; Narayanan, M.; Perumal, P. Highly efficient peroxidase-like activity of a metal-oxide-incorporated CeO 2-MIL (Fe) metal-organic framework and its application in the colorimetric detection of melamine and mercury ions via induced hydrogen and covalent bonds. *Analyst* **2022**, *147* (14), 3234−3247.
(10) Arunjegan, A.; Rajaji, P.; Sivanesan, S.; Panneerselvam, P. A Turn-ON fluorometric biosensor based on ssDNA immobilized with a metal phenolic nanomaterial for the sequential detection of Pb (ii) and epirubicin cancer drug. *RSC Adv.* **2021**, *11* (20), 12361−12373.
(11) Mandal, T.; Mishra, S. R.; Singh, V. Comprehensive Advances in Synthesis, Fluorescence Mechanism and Multifunctional Applications of Red-emitting Carbon Nanomaterials. *Nanoscale Advances* **2023**, *5*, 5717−5765.
(12) Sabei, F. Y. Colorimetric and fluorescent sensors based on nanomaterials for the detection of dipicolinic acid: a comprehensive review. *J. Nanopart. Res.* **2023**, *25* (12), 250.
(13) Xiao, K.; Zhu, R.; Zhang, X.; Du, C.; Chen, J. Ultrasensitive detection and efficient removal of mercury ions based on covalent organic framework spheres with double active sites. *Anal. Chim. Acta* **2023**, *1278*, 341751.
(14) Ji, Y.; Ni, C.; Jiang, Z.; Wu, N.; Qin, Y. Removal of mercury ions from water by triazine porous organic polymers rich in nitrogen and oxygen groups. *J. Mol. Struct.* **2024**, *1298*, 137066.
(15) Zhang, Y.; Huang, Y.; Miao, R.; Chen, H. Inorganic-Based Aggregation-Induced Luminescent Materials: Recent Advances and Perspectives. *Small Structures* **2023**, *4*, 2300157.
(16) Khorobrykh, F.; Bulatov, K.; Kutuza, I.; Zinin, P.; Kulnitskiy, B.; Goryunkov, A. A.; Lukonina, N. S.; Brotsman, V. A.; Galkin, A.; Popov, M. High pressure and high temperature phase transformations of covalent triazine-based frameworks. *Mater. Chem. Phys.* **2023**, *308*, 128312.
(17) Yang, L.; Song, Y.; Li, J.; Xu, W.; Peng, C.; Wang, L. S, N-rich luminous covalent organic frameworks for Hg2+ detection and removal. *Chemosphere* **2023**, *311*, 136919.
(18) Ma, J.; Shu, T.; Sun, Y.; Zhou, X.; Ren, C.; Su, L.; Zhang, X. Luminescent covalent organic frameworks for biosensing and bioimaging applications. *Small* **2022**, *18* (3), 2103516.
(19) Zhu, B.; Zhu, L.; Deng, S.; Wan, Y.; Qin, F.; Han, H.; Luo, J. A fully π-conjugated covalent organic framework with dual binding sites for ultrasensitive detection and removal of divalent heavy metal ions. *Journal of Hazardous Materials* **2023**, *459*, 132081.
(20) Ashraf, M.; Ullah, N.; Raziq, F.; Khan, I.; Alhooshani, K. R.; Ganiyu, S. A.; Tahir, M. N. Carbon Nitride (C3N3) Decorated with Non-Noble Metal Ni2P Co-Catalyst based Nanocomposites for Photocatalytic Water Splitting. *Electrochim. Acta* **2023**, *470*, 143296.
(21) Chaulagain, N.; Garcia, J.; Manoj, A.; Shankar, K. Ultrasensitive detection of Ag+ and Ce3+ ions using highly fluorescent carboxyl-functionalized carbon nitride nanoparticles. *Nanotechnology* **2024**, *35*, 315502.
(22) Fu, Y.; Yu, W.; Zhang, W.; Huang, Q.; Yan, J.; Pan, C.; Yu, G. Sulfur-rich covalent triazine polymer nanospheres for environmental mercury removal and detection. *Polym. Chem.* **2018**, *9* (30), 4125−4131.
(23) Huang, Y.; Feng, D.; Li, X.; Li, W.; Ren, J.; Zhong, H. Covalent organic frameworks assisted for food safety analysis. *Critical Reviews in Food Science and Nutrition* **2023**, 1−20.
(24) Shan, H.; Li, S.; Yang, Z.; Zhang, X.; Zhuang, Y.; Zhu, Q.; Cai, D.; Qin, P.; Baeyens, J. Triazine-based N-rich porous covalent organic polymer for the effective detection and removal of Hg (II) from an aqueous solution. *Chemical Engineering Journal* **2021**, *426*, 130757.
(25) Das, D.; Mitra, A.; Chatterjee, R.; Sain, S.; Chattopadhyay, K. K. A morphology-tailored triazine-based crystalline organic polymer for efficient mercury sensing. *New J. Chem.* **2019**, *43* (11), 4364−4376.
(26) Wang, Y.; Zhu, X.; Yang, M.; Ma, H.; Li, R.; Zhang, J.; Zhao, Q.; Ren, J.; Wang, X.; Yu, H. Fe Powder Catalytically Synthesized C3N3 toward High-Performance Anode Materials of Lithium-Ion Batteries. *ACS Appl. Mater. Interfaces* **2023**, *15* (18), 22051−22064.
(27) Liu, M.; Guo, L.; Jin, S.; Tan, B. Covalent triazine frameworks: synthesis and applications. *Journal of materials chemistry A* **2019**, *7* (10), 5153−5172.
(28) Cen, K.; Usman, M.; Shen, W.; Liu, M.; Yang, R.; Cai, J. A review on the assembly of multi-substituted pyridines via Co-catalyzed [2+ 2+ 2] cycloaddition with nitriles. *Organic & Biomolecular Chemistry* **2022**, *20* (37), 7391−7404.
(29) Chakrabortty, R.; Ghosh, S.; Ganesh, V. Ni0-Catalyzed Regioselective [2+ 2+ 2] Cyclotrimerization of 1, 3-Diynes: An Expeditious Synthesis of Hexasubstituted Alkynyl Benzenes. *Org. Lett.* **2024**, *26* (4), 792−797.
(30) Faghani, A.; Gholami, M. F.; Trunk, M.; Müller, J.; Pachfule, P.; Vogl, S.; Donskyi, I.; Li, M.; Nickl, P.; Shao, J. Metal-assisted and solvent-mediated synthesis of two-dimensional triazine structures on Gram Scale. *J. Am. Chem. Soc.* **2020**, *142* (30), 12976−12986.
(31) Salahvarzi, M.; Setaro, A.; Beyranvand, S.; Nemati, M.; Gordeev, G.; Fiebor, A.; Ludwig, K.; Ghanbari, R.; Nasiri, N.; Ahmadi, V. Room temperature synthesis of triazine covalent organic frameworks for size-selective intercalation of molecules and fast water purification. *Materials Today Chemistry* **2024**, *39*, 102155.
(32) Salahvarzi, M.; Setaro, A.; Ludwig, K.; Amsalem, P.; Schultz, T.; Mehdipour, E.; Nemati, M.; Chong, C.; Reich, S.; Adeli, M. Synthesis of two-dimensional triazine covalent organic frameworks at ambient conditions to detect and remove water pollutants. *Environmental Research* **2023**, *238*, 117078.
(33) Wang, D.-Y.; Wang, W.-J.; Wang, R.; Xi, S.-C.; Dong, B. A fluorescent covalent triazine framework consisting of donor-acceptor structure for selective and sensitive sensing of Fe3+. *Eur. Polym. J.* **2021**, *147*, 110297.
(34) Gujar, V.; Sangale, V.; Ottoor, D. A selective turn off fluorescence sensor based on propranolol-SDS assemblies for Fe 3+ detection. *J. Fluoresc.* **2019**, *29*, 91−100.
(35) Vijayan, A. P.; Ramakrishnan, K.; Elambalassery, J. G. Triazine-Adenine Anchored Porous Organic Polymer: An Integrated Approach as a Fluorescent Sensor and Molecular Sieve for Mercury Ions. *ACS Applied Polymer Materials* **2024**, *6* (7), 3975−3984.
(36) Ma, Q.; Liu, X.; Qian, J.; Zhuang, Q. Preparation of covalent organic framework with carboxy and triazine for efficient removal of Pb2+ ions. *Sep. Purif. Technol.* **2023**, *323*, 124368.
(37) Gonsalves, O. S.; Nemade, P. R. Ultrafast adsorption of hexavalent chromium from aqueous effluents using covalent triazine frameworks. *Chemosphere* **2024**, *351*, 141246.
(38) Ghazi, Z. A.; Khattak, A. M.; Iqbal, R.; Ahmad, R.; Khan, A. A.; Usman, M.; Nawaz, F.; Ali, W.; Felegari, Z.; Jan, S. U. Adsorptive removal of Cd 2+ from aqueous solutions by a highly stable covalent triazine-based framework. *New J. Chem.* **2018**, *42* (12), 10234−10242.
(39) Bilgic, A.; Cimen, A.; Kursunlu, A. N. Killing two birds with one stone": A fluorescent hybrid nanoparticle modified with BODIPY for efficiently detection and removal of toxic Cu (II) ion from aqueous solutions. *Science of The Total Environment* **2022**, *845*, 157170.
(40) Zhang, W.; Huang, Z.; Gao, Z.; Perez-Aguilar, J. M.; Gu, Z.; Tu, Y. Single atom catalysis for hydrogen evolution reaction using transition-metal atoms doped g-C3N3: A density functional theory study. *ChemistrySelect* **2023**, *8* (7), No. e202203475.
(41) Tang, S.; Liu, W.; Yang, Z.; Liu, C.; Bai, S.; Zhang, J.; Luo, D. Unveiling the anchoring and catalytic effect of Co@ C 3 N 3 monolayer as a high-performance selenium host material in lithium-selenium batteries: a first-principles study. *Phys. Chem. Chem. Phys.* **2023**, *25* (31), 21054−21064.

https://doi.org/10.1021/acsapm.4c01770
ACS Appl. Polym. Mater. 2024, 6, 11750−11761

(42) Ghashghaee, M.; Ghambarian, M.; Azizi, Z. Theoretical insights into sensing of hexavalent chromium on buckled and planar polymeric carbon nitride nanosheets of heptazine and triazine structures. *Mol. Simul.* **2020**, *46* (1), 54−61.
(43) Li, Z.; Feng, J.; Cao, J.; Jin, J.; Zhou, Y.; Cao, D.; Liang, Z.; Zhu, B.; Li, M.; Zhao, L. New carbon nitride C3N3 additive for improving cationic defects of perovskite solar cells. *Energy & Environmental Materials* **2023**, *6* (1), No. e12283.
(44) Zhang, Y.; Cao, Q.; Meng, A.; Wu, X.; Xiao, Y.; Su, C.; Zhang, Q. Molecular Heptazine-Triazine Junction over Carbon Nitride Frameworks for Artificial Photosynthesis of Hydrogen Peroxide. *Adv. Mater.* **2023**, *35* (48), 2306831.
(45) Song, Z.; Hou, J.; Raguin, E.; Pedersen, A.; Eren, E. O. u.; Senokos, E.; Tarakina, N. V.; Giusto, P.; Antonietti, M. Triazine-Based Graphitic Carbon Nitride Thin Film as a Homogeneous Interphase for Lithium Storage. *ACS Nano* **2024**, *18* (3), 2066−2076.
(46) Kumar, Y.; Ahmad, I.; Rawat, A.; Pandey, R. K.; Mohanty, P.; Pandey, R. Flexible Linker-Based Triazine-Functionalized 2D Covalent Organic Frameworks for Supercapacitor and Gas Sorption Applications. *ACS Appl. Mater. Interfaces* **2024**, *16* (9), 11605−11616.
(47) Panić, B.; Frey, T.; Borovina, M.; Konopka, K.; Sambolec, M.; Kodrin, I.; Biljan, I. Synthesis and characterization of benzene-and triazine-based azo-bridged porous organic polymers. *Polymers* **2023**, *15* (1), 229.
(48) Xu, Y.; Wu, C.; Chu, N.; Xing, Y.; Yang, J.; Yin, L.; Chen, X. Design and synthesis of stable sp2-carbon-linked two-dimensional conjugated covalent organic framework for efficient capture of iodine. *Sep. Purif. Technol.* **2023**, *307*, 122776.
(49) Wang, W.; Dong, W.; Ji, L.; Xia, Y.; Yang, S. Solubility of graphene-like two-dimensional layered C 3 N 3. *Chem. Commun.* **2022**, *58* (100), 13971−13974.
(50) Cui, W.-R.; Jiang, W.; Zhang, C.-R.; Liang, R.-P.; Liu, J.; Qiu, J.-D. Regenerable carbohydrazide-linked fluorescent covalent organic frameworks for ultrasensitive detection and removal of mercury. *ACS Sustainable Chem. Eng.* **2020**, *8* (1), 445−451.
(51) Merí-Bofí, L.; Royuela, S.; Zamora, F.; Ruiz-González, M. L.; Segura, J. L.; Muñoz-Olivas, R.; Mancheño, M. J. Thiol grafted imine-based covalent organic frameworks for water remediation through selective removal of Hg (II). *Journal of Materials Chemistry A* **2017**, *5* (34), 17973−17981.
(52) Liu, Q.; Yang, Y.; Zou, Y.; Wang, L.; Li, Z.; Wang, M.; Li, L.; Tian, M.; Wang, D.; Gao, D. Fluorescent covalent organic frameworks for environmental pollutants enriching and Sensing: A mini-review. *Analytical Methods* **2023**, *15* (44), 5919−5946.
(53) Oguz, M.; Gul, A.; Kursunlu, A. N.; Yilmaz, M. A bifunctional and multi-responsive fluorescent sensor for toxic analytes in the aqueous medium: Easy synthesis, NIR-visible effect, imaging in living cells. *J. Mol. Liq.* **2021**, *336*, 116861.
(54) Wang, Q.; Zhang, G.; Xing, W.; Pan, Z.; Zheng, D.; Wang, S.; Hou, Y.; Wang, X. Bottom-up Synthesis of Single-Crystalline Poly (Triazine Imide) Nanosheets for Photocatalytic Overall Water Splitting. *Angew. Chem.* **2023**, *135* (37), No. e202307930.
(55) Skorjanc, T.; Shetty, D.; Valant, M. Covalent organic polymers and frameworks for fluorescence-based sensors. *ACS sensors* **2021**, *6* (4), 1461−1481.
(56) Mohamed, M. G.; EL-Mahdy, A. F.; Kotp, M. G.; Kuo, S.-W. Advances in porous organic polymers: Syntheses, structures, and diverse applications. *Materials Advances* **2022**, *3* (2), 707−733.
(57) Kursunlu, A. N.; Bastug, E.; Oguz, A.; Oguz, M.; Yilmaz, M. A highly branched macrocycle-based dual-channel sensor: Bodipy and pillar [5] arene combination for detection of Sn (II) &Hg (II) and bioimaging in living cells. *Anal. Chim. Acta* **2022**, *1196*, 339542.
(58) Hong, H.; Wu, N.; Han, M.; Guo, Z.; Zhan, H.; Du, S.; Chen, B. An anthracene based conjugated triazine framework as a luminescent probe for selective sensing of p-nitroaniline and Fe (III) ions. *Materials Chemistry Frontiers* **2021**, *5* (17), 6568−6574.
(59) Tang, Y.; Huang, H.; Peng, B.; Chang, Y.; Li, Y.; Zhong, C. A thiadiazole-based covalent triazine framework nanosheet for highly selective and sensitive primary aromatic amine detection among various amines. *Journal of Materials Chemistry A* **2020**, *8* (32), 16542−16550.
(60) Liu, Y.; Wu, H.; Wang, Q. Strategies to improve the photocatalytic performance of covalent triazine frameworks. *Journal of Materials Chemistry A* **2023**, *11* (40), 21470−21497.
(61) Karbalaee Hosseini, A.; Tadjarodi, A. Novel Zn metal-organic framework with the thiazole sites for fast and efficient removal of heavy metal ions from water. *Sci. Rep.* **2023**, *13* (1), 11430.
(62) Gawas, P. P.; Selvaraj, K.; Pamanji, R.; Selvin, J.; Nutalapati, V. Highly sensitive fluorescence turn-OFF and reversible chemical sensor for Hg2+ ion based on pyrene appended 2-thiohydantoin. *Chemosphere* **2024**, *352*, 141470.
(63) Lai, S.; Jin, Y.; Shi, L.; Zhou, R.; Li, Y. Fluorescence Sensing Mechanisms of Versatile Graphene Quantum Dots toward Commonly Encountered Heavy Metal Ions. *ACS sensors* **2023**, *8* (10), 3812−3823.
(64) Shili, Q.; Xudong, H.; Fenglong, J.; Ying, W.; Hongtao, C.; Shuang, H.; Yangyang, S.; Lidi, G. A facile imine-linked covalent organic framework doped with a carbon dot composite for the detection and removal of Hg 2+ in surface water. *RSC Adv.* **2022**, *12* (29), 18784−18793.
(65) Masoumi, H.; Ghaemi, A.; Gilani, H. G. Evaluation of hyper-cross-linked polymers performances in the removal of hazardous heavy metal ions: A review. *Sep. Purif. Technol.* **2021**, *260*, 118221.
(66) Bilgic, A.; Cimen, A.; Bastug, E.; Kursunlu, A. N. Fluorescent sporopollenin microcapsule modified by BODIPY for sensitive & selective recognition and efficient removal of Cu (II) from aqueous solution. *Chem. Eng. Res. Des.* **2022**, *178*, 61−72.
(67) Zuo, S.; Sun, Y.; Zheng, Y.; Sun, X.; Hu, J. Efficient selective uptake of Hg (II) using a porous organic polymer rich in N and S atoms. *Journal of Environmental Chemical Engineering* **2024**, *12* (1), 111924.
(68) Wang, L.; Song, Y.; Luo, Y.; Wang, L. A novel covalent organic framework with multiple adsorption sites for removal of Hg2+ and sensitive detection of nitrofural. *Journal of Industrial and Engineering Chemistry* **2022**, *106*, 374−381.
(69) Fu, Q.; Zhang, T.; Sun, X.; Zhang, S.; Waterhouse, G. I.; Sun, C.; Li, H.; Ai, S. Pyridine-based covalent organic framework for efficient and selective removal of Hg (II) from water: Adsorption behavior and adsorption mechanism investigations. *Chemical Engineering Journal* **2023**, *454*, 140154.
(70) Elbayoumy, E.; Elhendawy, M.; Gaafar, M. M.; Moawed, E. Novel fluorescent sensor based on triazole-pyridine derivative for selective detection of mercury (II) ions in different real water samples: Experimental and DFT calculations. *J. Mol. Liq.* **2024**, *401*, 124589.

https://doi.org/10.1021/acsapm.4c01770
ACS Appl. Polym. Mater. 2024, 6, 11750−11761